Supporting information for the paper "Detailed characterization of a nanosecond-lived excited state: X-ray and theoretical investigation of the quintet state in photoexcited $[Fe(terpy)_2]^{2+}$"

György Vankó,[*,†] Amélie Bordage,[†,‡‡] Mátyás Pápai,[†] Kristoffer Haldrup,[‡] Pieter Glatzel,[¶] Anne Marie March,[§] Gilles Doumy,[§] Alexander Britz,[∥,⊥] Andreas Galler,[∥] Tadesse Assefa,[∥] Delphine Cabaret,[#] Amélie Juhin,[#] Tim B. van Driel,[‡] Kasper S. Kjær,[‡,@] Asmus Dohn,[△] Klaus B. Møller,[△] Henrik T. Lemke,[▽] Erik Gallo,[¶] Mauro Rovezzi,[¶] Zoltán Németh,[†] Emese Rozsályi,[†] Tamás Rozgonyi,[††] Jens Uhlig,[@] Villy Sundström,[@] Martin M. Nielsen,[‡] Linda Young,[§] Stephen Southworth,[§] Christian Bressler,[∥,⊥] and Wojciech Gawelda[∥]

E-mail: vanko.gyorgy@wigner.mta.hu

1. Correlation table for the symmetry groups of $[Fe(terpy)_2]^{2+}$

Table S1: Correspondence between the notation of the relevant electronic states for the point group symmetries used in the paper.

O_h point group	D_{2d} point group	C_2 point group
$^1A_{1g}$	$^1A_1$	$^1A(1)$
$^1T_{1g}$	$^1A_2$	$^1A(2)$
	^1E	$^1B(1)$
		$^1B(2)$
$^3T_{1g}$	$^3A_2$	$^3A(1)$
	$^3E(1)$	$^3B(1)$
		$^3B(2)$
$^3T_{2g}$	$^3B_1$	$^3A(2)$
	$^3E(2)$	$^3B(3)$
		$^3B(4)$
$^5T_{2g}$	$^5B_2$	$^5A(1)$
	^5E	$^5B(1)$
		$^5B(2)$
^5E_g	$^5B_1$	$^5A(2)$
	$^5A_2$	$^5A(3)$

2. XAFS data quality

The unprecedented quality of our time-resolved X-ray absorption data is demonstrated

*To whom correspondence should be addressed

†Wigner Research Centre for Physics, Hungarian Academy Sciences, H-1525 Budapest, P.O.B. 49., Hungary

‡Centre for Molecular Movies, Technical University of Denmark, Department of Physics, DK-2800, Kgs. Lyngby, Denmark

¶European Synchrotron Radiation Facility (ESRF), 6 Rue Jules Horowitz, BP220, 38043 Grenoble Cedex 9, France

§X-ray Science Division, Advanced Photon Source, Argonne National Laboratory, 9700 S. Cass Ave., Argonne, Illinois 60439, USA

‖European XFEL, Albert-Einstein Ring 19, D-22761 Hamburg, Germany

⊥The Hamburg Centre for Ultrafast Imaging, Luruper Chaussee 149, 22761 Hamburg, Germany

#Université Pierre et Marie Curie, IMPMC, UMR CNRS 7590, 4 place Jussieu, 75252 Paris Cedex 05, France

@Dept. of Chemical Physics, Lund University, Box 124, 22100 Lund, Sweden

△Centre for Molecular Movies, Technical University of Denmark, Department of Chemistry, DK-2800, Kgs. Lyngby, Denmark

▽SLAC National Accelerator Laboratory, Linac Coherent Light Source, Menlo Park, California 94025, USA

††Research Centre for Natural Sciences, Hungarian Academy of Sciences, H-1519 Budapest, P.O. Box 286, Hungary

‡‡Present address: Université Paris-Sud, ICMMO UMR 8182, Equipe de Chimie Inorganique, 91405 Orsay, France

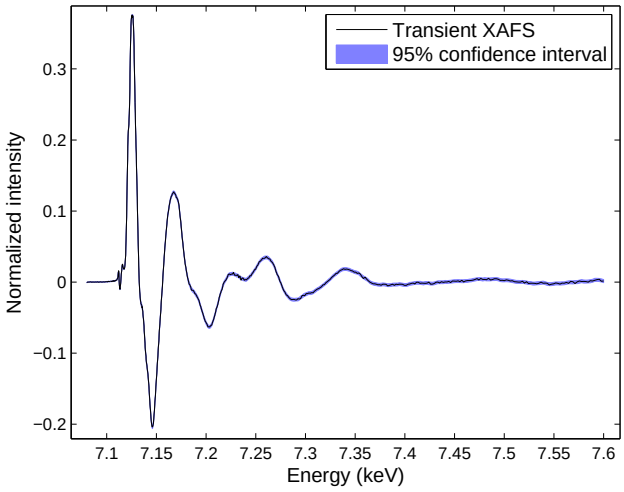

Figure S1: Transient XAS spectrum of $[Fe(terpy)_2]^{2+}$ (i.e. laser excited – ground state).

in Fig. S1. The data was collected during 5 hours, in a repetitive 1 bunch laser ON / 4 bunch laser OFF pattern. This means that only 1 hour was effectively used to record laser-excited data, accumulating 7×10^8 counts. The data has been summed up and normalized without any smoothing.

3. **Lifetime fitting**

In the Fe *1s* XAS, as seen in Fig. S1, the 7125 eV feature shows the largest variation at the spin transition. The time evolution of the photoexcited sample was measured by recording the intensity of this feature. For each time delay setting, the acquisition alternated between measuring the signal with and without the laser excitation. These are shown in Fig. S2. The data have been corrected to eliminate artefacts emerging from the laser phase shifter and the corrected ratio has been fitted with Eq. S1.

Figure 3 of the paper displays the time evolution of the intensity of this signal feature, which corresponds to the formation and decay of the HS state. The width of the rise centered at $\Delta t = 0$ corresponds to the X-ray probe pulse width (≈80 ps), while the later exponential decay is governed by the lifetime of the HS state. This time evolution is fitted by an expression of the form

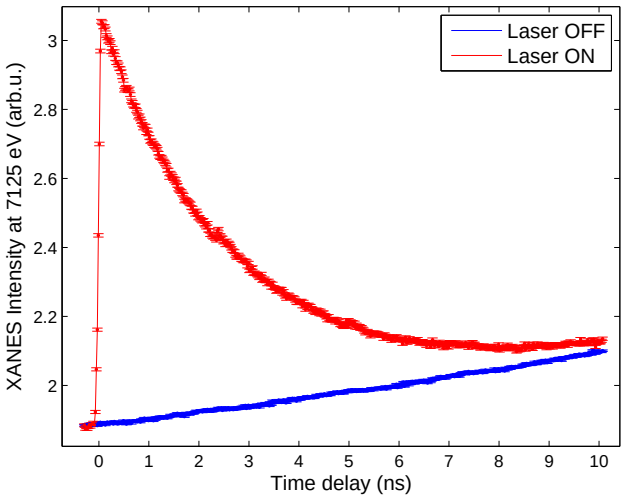

Figure S2: Time evolution of the intensity of the 7125 eV feature of the $[Fe(terpy)_2]^{2+}$ XANES spectrum with and without laser excitation as a function of the time delay between the laser and the X-ray pulses.

$$I(\Delta t) = I(t - t_0) = \gamma_0 \int_{-\infty}^{\infty} \frac{1}{\sigma\sqrt{2\pi}} e^{-y^2/2\sigma^2} H(t - t_0 - y) e^{-(t-t_0-y)/\tau} dy + C \qquad \text{(S1)}$$

derived from a Gaussian broadening of an exponential decay starting at $\Delta t = 0$. τ stands for the lifetime of the HS state, t_0 is the time of the laser excitation, and H is the heaviside step function, and C is the background.

Table S2: Parameters for fitting Eq. S1 to the delay-dependent 7125 eV XANES intensity.

τ	2.612 $\pm$0.006 ns
σ	0.0323* $\pm$0.0004 ns
t_0	-0.0075 ± 0.0003 ns
γ_0	0.4157 ± 0.0004
C	0.0009 ± 0.0004

$*$ FWHM: 76.2 ± 0.9 ps

A large correlation was only observed between the lifetime and the background: $\text{correl}(\tau, C) = -0.82$.

4. **EXAFS data reduction and fitting**

This section describes the details of the EXAFS data reduction and subsequent fitting procedure for both LS and HS spectra, which are shown in Fig. 4 of the paper.

As explained in the Theoretical Methods section of the paper, Density Functional Theory (DFT) has been applied to obtain the molecular structures of both the LS $^1A_1$ ground state (Fig. S3A) and two possible lowest energy HS states, namely $^5B_2$ (Fig. S3B) and ^5E (Fig. S3C) quintets. (We have used Mercury CSD 2.0 software[1] for plotting the DFT-optimized structures shown in Figs. S3 and S4.)

Note that the ^5E undergoes a Jahn-Teller distortion, and its symmetry lowers to C_2. In this point group the correct notation for ^5E would be ^5B, but we keep the higher symmetry notation (^5E) in order to avoid confusion with the state $^5B_2$.

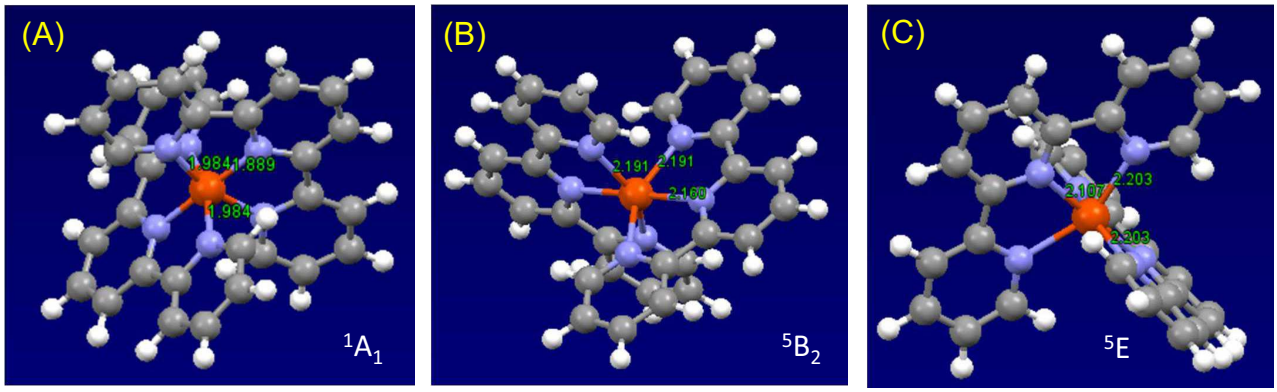

Figure S3: The atomic structures of the $^1A_1$ (A), and $^5B_2$ (B) and ^5E (C) metal-centered states of aqueous $[Fe(terpy)_2]^{2+}$ complex as predicted by DFT.

Due to the steric constraints imposed by terpyridine ligands, the N atoms of pyridine rings cannot be accommodated in ideal octahedral positions around the Fe atom, which results in a distorted geometry for the LS $^1A_1$ ground state with two different types of coordinating nitrogen atoms: 4 N atoms lie in the equatorial plane (N_{eq}) and the remaining 2 N atoms (N_{ax}) are on the molecular axis (Fig. S4A). The axial bond lengths R(Fe–N_{ax}) are about 0.1 Å shorter than the equatorials (R(Fe–N_{eq})), thus the molecule is axially compressed. For the ^5E quintet state, DFT calculations predict a fairly similar bond elongation for both axial and equatorial directions, preserving the

LS axial compression. On the contrary, for the $^5B_2$ quintet state the bond elongation in the axial direction is expected to be 0.05 Å larger than in equatorial direction[2] thus the Fe–N bond lengths become almost uniform, as can be seen in Fig. S4B.

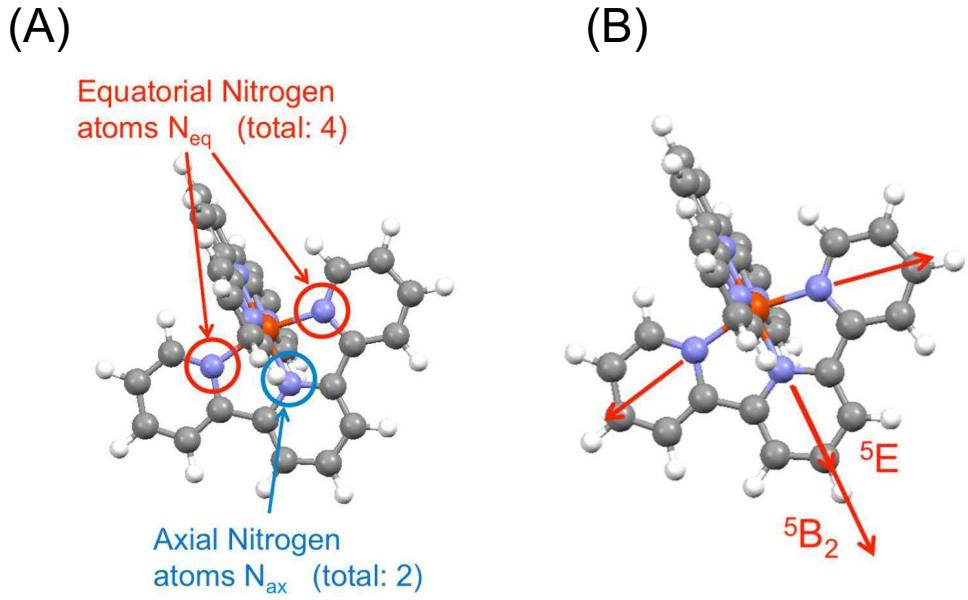

Figure S4: The effect of geometrical constraints, due to the nature of tridentate terpyridine, is shown for $^1A_1$ (A) and $^5B_2$ / ^5E geometries (B). The red and blue circles in (A) mark the positions of equatorial and axial N atoms, respectively. The red arrows in (B) indicate the structural distortion of Fe-ligand bonds (bond expansion) in the two possible quintet states.

Using structural models for ground and both possible excited states (ES), EXAFS spectra have been simulated and fitted using FEFF[3] and IFEFFIT[4] codes, respectively. The calculations of scattering amplitudes and phases were carried out using the FEFF8.20 code. The atomic potentials were calculated self-consistently within the muffin-tin approximation and the Hedin-Lundqvist self-energy model was chosen as an exchange correlation potential for both the fine structure and the atomic background.

The experimental EXAFS spectrum of the ground state (GS) was reduced using the Athena program (part of IFEFFIT package). The data reduction consisted of normalization and removal of the atomic background μ_0 using a cubic spline function. Once reduced, the GS EXAFS spectrum was fitted with the Artemis software (also part of IFEFFIT) using the scattering amplitudes and phases calculated by FEFF8.20 for

$^1A_1$ geometry (Fig. S3A). All fits were performed in R-space using k^2 weighting and the results are summarized in Table S3. We have used identical k ranges for Fourier transforms of both LS and HS spectra (2.5–10.5 Å^{-1}) and identical R ranges (1-3.8 Å) for both fits presented in Fig. 4 of the paper. This resulted in the same number of statistically independent data points $N_i = (2\Delta k \Delta R)/\pi$, where Δk and ΔR are the ranges in k- and R-space, respectively. The fit evaluation was done using a standard statistical χ^2 function and the confidence limits for fit parameters were estimated using the error estimation method described in Refs 5,6. One should note that the number of degrees of freedom $\nu = N_i - P$, where P is the maximum number of parameters used in the fit, was different for LS and HS fits and the corresponding values are reported in Table S3.

Table S3: EXAFS fit results for the LS and photoexcited HS states of $[Fe(terpy)_2]^{2+}$ in solution.

	LS (A_1)	HS
R(Fe–N_{ax})	1.874(4) Å	2.08(2) Å
R(Fe–N_{eq})	1.969(4) Å	2.20(1) Å
S_0^2	0.78(4)	0.78(4)
$\sigma^2(R$(Fe–N))	$2.6(7) \times 10^{-3}$ Å^2	$2.6(7) \times 10^{-3}$ Å^2
E_0	−5.8(4) eV	−4.0(7) eV
N_i	14	14
ν	6	9
χ^2	165	315
Reduced χ_r^2	28	35
R-factor	0.1 %	1.1 %

We have optimized the change in Fe–N bond lengths for axial (Fe–N_{ax}) and equatorial (Fe–N_{eq}) N atoms by one value, next to the change in second-shell Fe–C bond distances and the change in additional further lying single and multiple scattering shells of C atoms (not shown in the table).

We have constrained the changes in Fe–N bond lengths for two ΔR values: one for the axial (Fe–N_{ax}) and one for the equatorial (Fe–N_{eq}) bonds, while using one parameter for the change in second-shell Fe–C bond distances and the one for the change in

additional further lying single and multiple scattering shells of C atoms (not shown in the table).

For each coordination shell we have obtained a Debye-Waller (DW) factor and we have used a global value of the energy threshold (E_0) and amplitude reduction factor (S_0^2) for all scattering contribution of the GS spectrum, which results in a maximum number of fit parameters $P = 8$. The fit was done by optimizing all variables simultaneously. The results for the GS spectrum show a very good agreement with the geometry of the LS $^1A_1$ state with only small corrections to the Fe–N_{ax} and Fe–N_{eq} bond lengths. We have not observed any significant parameter correlations for multi-shell fitting. Therefore we concluded that the DFT-predicted atomic structure of the singlet LS state provides a good structural model of the GS $[Fe(terpy)_2]^{2+}$ complex.

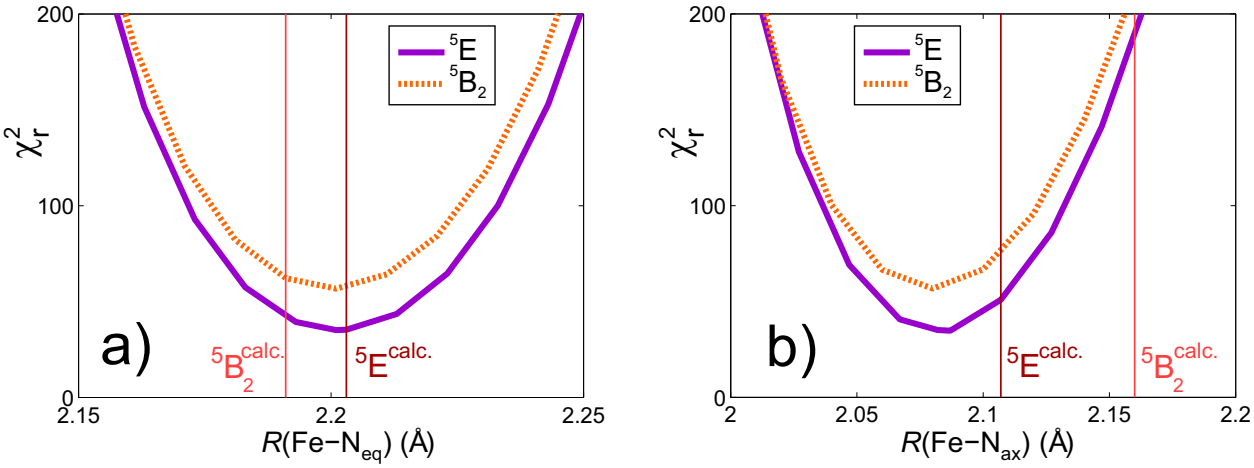

Figure S5: Square residuals between the experimental excited state EXAFS data and ^5E and $^5B_2$ model geometries of the HS quintet state as a function of Fe–N_{ax} *(left)* and Fe–N_{eq} *(right)* bond distances. All other EXAFS fit parameters were fixed during the analysis. The dotted vertical lines indicate the predicted axial and equatorial Fe–N bond lengths as obtained by DFT.

The quintet EXAFS spectrum was reconstructed from the transient difference spectrum and the LS spectrum using a relation described in Ref. 7 and the excited HS state fraction derived from XES measurements (see main text for details). In order to minimize the number of systematic errors introduced by data normalization and

reduction procedures, we have used the GS μ_0 function to normalize and remove the background from the ES spectrum using a Matlab code. Fitting of the ES EXAFS spectrum was carried out similarly to the GS case, and we have fixed DW factors and S_0^2 in order to minimize the free parameter space in the fitting procedure. The E_0 parameter was constrained in the fit to vary in a limited range, as it is strongly correlated with Fe–N bond distance changes. Fits using both $^5B_2$ and ^5E atomic coordinates as initial parameters were performed in R-space, with the same k^2-weighting as for the GS spectrum and using the same number of statistically independent data points, i.e. $N_i = 14$. As mentioned earlier, only the energy shift E_0 and the changes in bond lengths, for Fe–N_{ax} and Fe–N_{eq} separately, as well as small corrections to the second shell Fe–C distances and to all longer scattering paths, were optimized, which resulted in $P = 5$. The summary of the most relevant fit results including statistical parameters used in the estimation of the fit errors is presented in Table S3.

We have performed fitting using both $^5B_2$ and ^5E input geometries independently as initial guesses. The fit results converged to an identical HS state model, which was very close to the DFT-predicted ^5E structure. Therefore we conclude that the measured ES EXAFS spectrum resembles closely the ^5E geometry of the aqueous $[Fe(terpy)_2]^{2+}$ obtained by DFT, independent of the initial structural model used for FEFF8 simulations and with only minor changes in the relevant Fe–N_{ax}, Fe–N_{eq} bond distances and for higher coordination shells. The observed red-shift of $\Delta E_0 = -1.8$ eV is also in agreement with what has been observed earlier for similar spin-transition complexes, which reflects the expansion of the Fe–ligand bonds.[8,9]

Since the structural differences between $^5B_2$ and ^5E geometries are very subtle, only due to the very high quality of our EXAFS data and a precise reconstruction of the HS EXAFS spectrum (using a very accurate measure of the photoexcited HS fraction derived from XES spectrum) was it possible to distinguish both models with statistically relevant accuracy. As mentioned earlier, standard χ^2 tests were also used to

evaluate and compare the statistical goodness of the EXAFS fits as a function of the most relevant structural parameters, namely Fe–N_{ax} and Fe–N_{eq} bond distances. Here, we have varied the Fe–N_{ax} bond lengths in small steps of 0.02 Å and the Fe–N_{eq} bond lengths in steps of 0.01 Å and let the rest of the molecular structure relax with DFT. With fixed values for all remaining fit parameters (including E_0 and DW factors), we calculated the corresponding reduced $\chi_r^2 = \chi^2/\nu$ residual using the experimental and the calculated EXAFS spectrum of both $^5B_2$ and ^5E models. These results are shown in Fig. S5. As can be seen in the figure, in both cases a minimum χ_r^2 value is reached; however, it always leads to significantly smaller values for the ^5E starting geometry, as compared to $^5B_2$. For comparison, we have plotted the DFT-optimized values for Fe–N_{ax} and Fe–N_{eq}, which are represented by vertical lines in Figs. S5A and S5B, respectively. We observe a consistent result by comparing the DFT-calculated Fe–N bond distances with the best-fit value, as the ^5E geometry is closest for both axial and equatorial N positions to the minimum χ_r^2 positions obtained in our analysis.

5. **Diagrams of Kohn-Sham spin-unrestricted molecular orbitals**

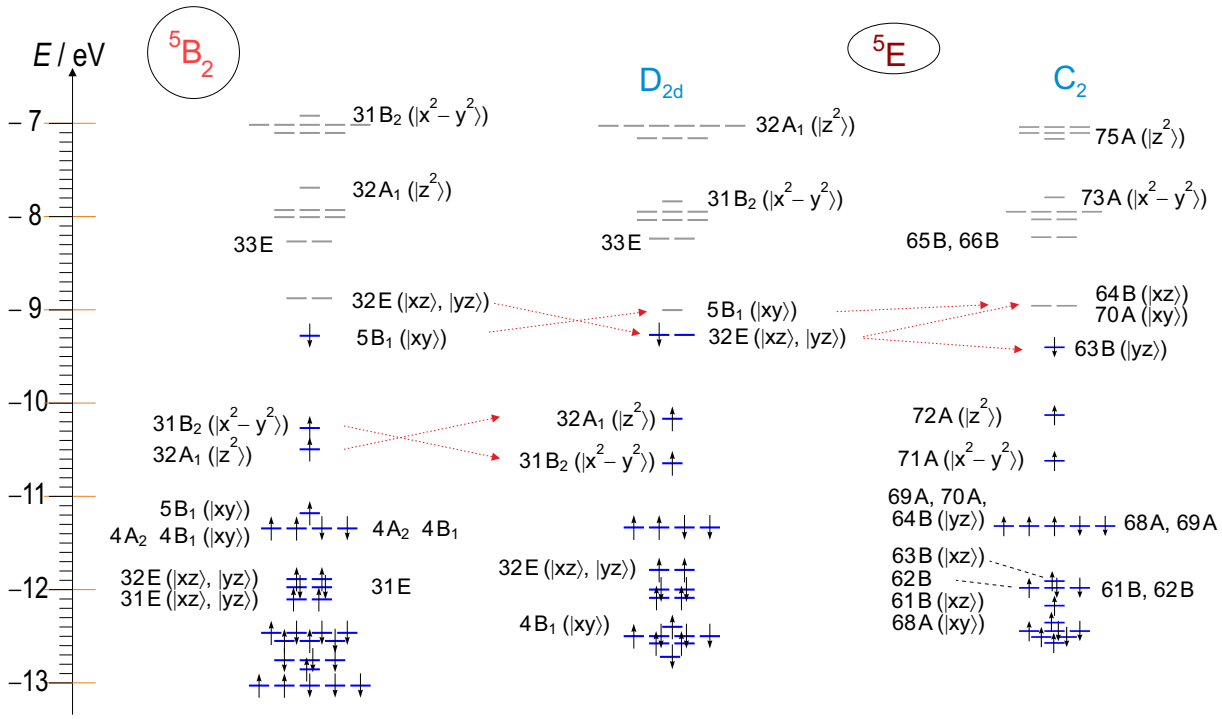

Figure S6: A molecular orbital diagram of the quintet states of $[Fe(terpy)_2]^{2+}$, a more detailed version of Fig. 8 in the main text. α orbital symbols are left, β are right of the orbital energy levels; those containing relevant $3d$-contribution are noted in parenthesis). Both the highly symmetric (D_{2d}), and Jahn-Teller distorted (C_2) states are shown for the ^5E (similarly to Fig. 8.)

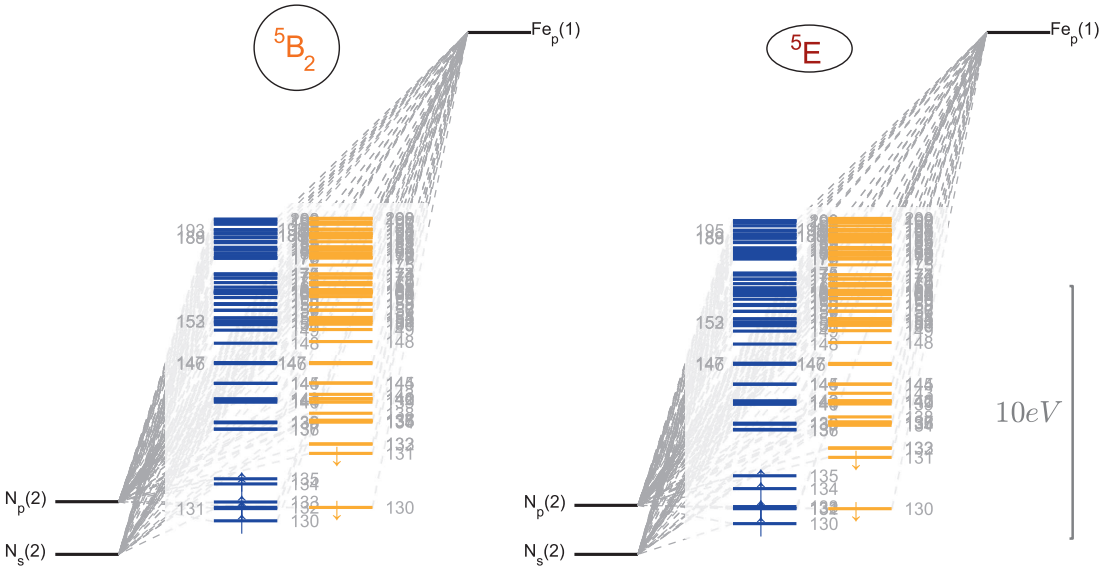

Figure S7: Energy diagram of the DFT-calculated molecular orbitals with Fe p-orbital contributions of $[Fe(terpy)_2]^{2+}$ for the two quintet states; blue and yellow denotes α (spin-up) and β (spin-down) orbitals, respectively. The apparent similarity for the struture and density of the unoccupied state levels in the two states suggest that their absorption spectra must be very similar.

References

(1) Macrae, C. F.; Bruno, I. J.; Chisholm, J. A.; Edgington, P. R.; McCabe, P.; Pidcock, E.; Rodriguez-Monge, L.; Taylor, R.; van de Streek, J.; Wood, P. A. *Journal of Applied Crystallography* **2008**, *41*, 466–470.

(2) Pápai, M.; Vankó, G.; de Graaf, C.; Rozgonyi, T. *Journal of Chemical Theory and Computation* **2013**, *9*, 509–519.

(3) Ankudinov, A. L.; Ravel, B.; Rehr, J. J.; Conradson, S. D. **1998**, *58*, 7565–7576.

(4) Ravel, B.; Newville, M. *Journal of Synchrotron Radiation* **2005**, *12*, 537–541.

(5) Lytle, F. W.; Sayers, D. E.; Stern, E. A. *Physica B: Condensed Matter* **1989**, *158*, 701 – 722.

(6) International X-ray Absorption Society (IXS) Standards and Criteria Report: Error Reporting Recommendations. `http://ixs.iit.edu/subcommittee_reports/sc/err-rep.pdf`.

(7) Bressler, C.; Chergui, M. *Chemical Reviews* **2004**, *104*, 1781–1812.

(8) Gawelda, W.; Pham, V.-T.; van der Veen, R. M.; Grolimund, D.; Abela, R.; Chergui, M.; Bressler, C. *The Journal of Chemical Physics* **2009**, *130*, 124520.

(9) Huse, N.; Kim, T. K.; Jamula, L.; McCusker, J. K.; de Groot, F. M. F.; Schoenlein, R. W. *Journal of the American Chemical Society* **2010**, *132*, 6809–6816.